



**HAL**  
open science

## Encapsulation of Microperoxidase-8 in MIL-101(Cr)-X Nanoparticles: Influence of Metal-Organic Framework Functionalization on Enzymatic Immobilization and Catalytic Activity

Effrosyni Gkaniatsou, Rémy Ricoux, Kalani Kariyawasam, Ingrid Stenger, Benhui Fan, Narjès Ayoub, Samanta Salas, Gilles Patriarche, Christian Serre, Jean Pierre Mahy, et al.

### ► To cite this version:

Effrosyni Gkaniatsou, Rémy Ricoux, Kalani Kariyawasam, Ingrid Stenger, Benhui Fan, et al.. Encapsulation of Microperoxidase-8 in MIL-101(Cr)-X Nanoparticles: Influence of Metal-Organic Framework Functionalization on Enzymatic Immobilization and Catalytic Activity. ACS Applied Nano Materials, 2020, 3 (4), pp.3233-3243. 10.1021/acsanm.9b02464 . hal-02677097

**HAL Id: hal-02677097**

**<https://hal.science/hal-02677097v1>**

Submitted on 15 Jan 2021

**HAL** is a multi-disciplinary open access archive for the deposit and dissemination of scientific research documents, whether they are published or not. The documents may come from teaching and research institutions in France or abroad, or from public or private research centers.

L'archive ouverte pluridisciplinaire **HAL**, est destinée au dépôt et à la diffusion de documents scientifiques de niveau recherche, publiés ou non, émanant des établissements d'enseignement et de recherche français ou étrangers, des laboratoires publics ou privés.

# **Encapsulation of Microperoxidase-8 in MIL-101(Cr)-X Nanoparticles: Influence of MOF Functionalization on Enzymatic Immobilization and Catalytic Activity**

*Effrosyni Gkaniatsou<sup>†</sup> Rémy Ricoux<sup>‡\*</sup> Kalani Kariyawasam,<sup>‡</sup> Ingrid Stenger,<sup>§</sup> Benhui Fan,<sup>†</sup> Narjès Ayoub,<sup>†</sup> Samanta Salas,<sup>†</sup> Gilles Patriarche,<sup>±</sup> Christian Serre,<sup>¶</sup> Jean-Pierre Mahy,<sup>‡</sup> Nathalie Steunou,<sup>†</sup> and Clémence Sicard<sup>†\*</sup>*

<sup>†</sup> Institut Lavoisier de Versailles, UVSQ, CNRS, Université Paris-Saclay, Versailles, France.

<sup>‡</sup>Laboratoire de Chimie Bioorganique et Bioinorganique, Institut de Chimie Moléculaire et des Matériaux d'Orsay, UMR 8182, Université Paris Sud, Université Paris-Saclay, Orsay, France.

<sup>§</sup>Groupe d'étude de la matière condensée, UVSQ, CNRS, Université Paris-Saclay, Versailles, France.

<sup>±</sup> Université Paris-Saclay, CNRS, Centre de Nanosciences et de Nanotechnologies, 91120, Palaiseau, France.

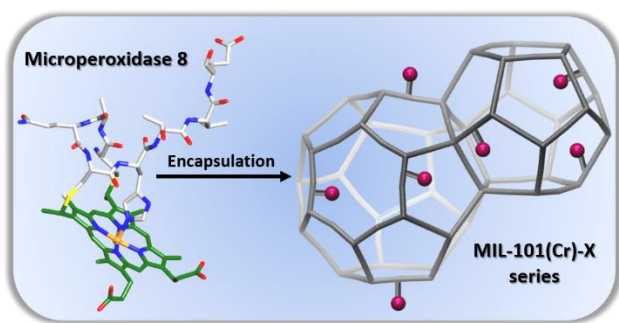
<sup>¶</sup>Institut des Matériaux Poreux de Paris, , UMR 8004 CNRS Ecole Normale Supérieure, Ecole Supérieure de Physique et de Chimie Industrielles de Paris, PSL research university, Paris, France.

**Keywords:** Metal-Organic Frameworks, enzyme, immobilization

## Abstract

Microperoxidase 8 (MP8) was immobilized within MIL-101(Cr) bearing terephthalate linkers with functionalized groups (-NH<sub>2</sub> and -SO<sub>3</sub>H). A synthesis protocol for MIL-101(Cr)-SO<sub>3</sub>H that avoids the use of toxic Cr(VI) and HF was developed. The electrostatic interactions between the MP8 molecules and the MOF matrices were found to be crucial for a successful immobilization. Raman spectroscopy revealed the dispersion of the immobilized MP8 molecules in MIL-101(Cr)-X matrices as monomers without aggregation. The presence of functional groups resulted in higher amounts of immobilized MP8 in comparison to the bare MIL-101(Cr). The catalytic activity of MP8@MIL-101(Cr)-NH<sub>2</sub> per material mass was higher than for MP8@MIL-101(Cr). The presence of free amino groups can thus improve the immobilization efficiency, leading to higher amount of catalytic active species and improving the subsequent catalytic activity of the heterogeneous biocatalysts. MP8@MIL-101(Cr)-NH<sub>2</sub> successfully catalyzed as well the selective oxidation of thioanisole derivatives into sulfoxides.

## Table of Contents artwork



## Introduction

Biocatalytic applications exhibit many advantages as enzymes are often highly selective with high turn-over numbers. They derive from natural sources and operate under ambient temperature, atmospheric pressure and aqueous solutions, which allow for green cost-effective processes. However, a drawback of enzymes is their often low operational stability<sup>1</sup> and their difficult recovery and reusability that may hamper their application. These problems can be circumvented by their immobilization on solid supports, which provides the benefits of heterogeneous catalysis (recycling, shaping...) and may protect the enzymes from operational conditions (high temperature, pH, solvent). Traditional inorganic and organic supports (sol-gel glasses, biopolymers, synthetic polymers,) have been used to enhance enzymatic activities.<sup>2-4</sup> The combination of several materials may however be required to obtain hybrid matrices that address stability and leaching issues.<sup>5,6</sup> Besides, most of these materials do not present any long-range order, thereby limiting any control over the distribution of enzymes.

Recently, Metal-Organic Frameworks (MOFs), a class of hybrid crystalline porous materials, have been highlighted as promising immobilization matrices.<sup>7,8</sup> MOFs are built-up from the assembly of inorganic units and polytopic organic ligands. They combine the advantages of organic and inorganic supports, providing specific interactions with enzymes and robust structures. Several immobilization techniques have been developed,<sup>9-12</sup> but the entrapment of enzymes inside the porosity of preformed MOFs (*i.e.* cage inclusion) has been largely preferred for biocatalytic applications, since the 3D confinement of enzymes provides enhanced protection and stabilization.<sup>13-15</sup> Moreover, the high surface area and regular porosity of MOFs can ensure homogeneous

immobilization of biomolecules with high loadings. For the selection of MOF matrices for the cage inclusion of enzymes, three main criteria appeared as critical. The size matching between the enzyme and the pores apertures is a prerequisite for a successful immobilization. The presence of interconnected hierarchical porosity that allows the confinement of enzymes in larger pores, while preserving a free porosity for the diffusion of substrates, was shown to lead to biocatalysts with superior performances than isolated 1-D channel porous system.<sup>16</sup> Also, MOF nanoparticles have been shown to favour substrate diffusion compared to micron-sized MOFs.<sup>17</sup> Finally, the impact of the hydrophilic/hydrophobic nature of the framework on the catalytic activity of the entrapped enzyme was reported.<sup>18</sup> However, the influence of pending functional groups in MOF frameworks on the stability and activity of encapsulated enzymes has been rarely investigated. Functional groups may promote stabilizing interactions between the MOF and the enzyme, enabling higher loadings and/or enhancing the catalytic activity.

In this work, Microperoxidase 8 (MP8) that derives from the hydrolytic digestion of horse cytochrome c (Cyt c) was selected. It contains a heme prosthetic group covalently attached to an octapeptide with amino acid residues 14 to 21 of Cyt c (**Fig. S1**). MP8 possesses a dual catalytic activity (a peroxidase- and a Cytochrome P450-like activity) that allows the selective oxidation of organic molecules in water, including organosulfur compounds.<sup>19</sup> However, the catalytic activity of MP8 is usually hampered by high concentrations of H<sub>2</sub>O<sub>2</sub> and acidic conditions.<sup>20,21</sup> We have recently demonstrated that MP8 encapsulation in nanoparticles of MIL-101(Cr) enabled its protection and stabilization, under these conditions.<sup>22</sup> MIL-101(Cr) has a high hierarchical, interconnected mesoporosity (cages of 2.9 nm and 3.4 nm) (**Fig. S1**), compatible with the

size of MP8 ( $<3.3 \times 1.1 \times 1.7$  nm) and once the enzyme is immobilized, part of the porosity remains accessible for the diffusion of substrates. Herein, we focused on nanoparticles of functionalized MIL-101(Cr) analogues with terephthalate linkers bearing hydrophilic substituents to induce a good affinity with the hydrophilic MP8 enzyme.<sup>18,23</sup> MIL-101(Cr)-NH<sub>2</sub> was selected as the amino groups could lead to favourable interactions with the four free carboxylic acid groups of MP8 (**Fig. S1**),<sup>24</sup> and it was recently shown to favour interactions for enzyme translocation into MOF.<sup>25</sup> For comparison's sake, MIL-101(Cr)-SO<sub>3</sub>H bearing sulfonate functionalized terephthalate linkers was also studied, since it may interact differently with the substituents of MP8. In order to probe the influence of the MOFs functional groups, MP8 was encapsulated in the three MIL-101(Cr)-X (X = H, NH<sub>2</sub> and SO<sub>3</sub>H). The corresponding MP8@MIL-101(Cr)-X materials were structurally characterized, and Raman spectroscopy was employed to probe the MP8 molecules conformation after their immobilization. The catalytic activities of the three MP8@MIL-101(Cr)-X were compared toward a typical peroxidase substrate, along with the protective effect of the MOF matrices against acidic conditions.

Most of MOF-enzyme materials have mainly been studied for the biocatalysis of model reactions, with typical chromogenic substrates (e.g. 3,5-dit-butyl-catechol (DTBC), p-nitrophenyl butyrate (PNPB), 2,2'-azino-bis(3-ethylbenzothiazoline-6-sulphonic acid) (ABTS), etc...).<sup>13,16,26</sup> Only very recently, more challenging reactions such as nerve agent detoxification<sup>27</sup> and tumor specific prodrug activation<sup>28</sup> have been reported. It was thus of interest to investigate the catalytic activity of MP8 encapsulated in MIL-101(Cr)-X toward a more challenging reaction such as sulfoxidation. Organosulfur compounds are common pollutants of wastewater and fossil fuel. Their presence in the latter is a

significant issue as their combustion results in the emission of toxic SO<sub>x</sub> compounds. Therefore, desulfurization is often required and vast research has been conducted on this topic.<sup>29,30</sup> Among the developed techniques, oxidation of organosulfur has appeared as a sustainable process that can yield sulfones compounds, which are of great importance for the synthesis of fine chemicals, biologically active compounds, chiral auxiliaries etc...<sup>31-</sup>  
<sup>34</sup> A variety of catalysts has been employed over the years for such transformations, like polyoxometallates,<sup>35</sup> Schiff-base complexes<sup>36</sup> and titanium oxide.<sup>37</sup> Among them, enzymes, such as peroxidases represent a very promising class of bio-catalysts, as they combine environmentally friendly operational conditions and high selectivity.<sup>38,39</sup> More specifically, we targeted the selective oxidation by free and immobilized MP8 of the sulfides family of thioanisole derivatives, differing by their substituting groups (-H, -OCH<sub>3</sub>, -CH<sub>3</sub> and -NO<sub>2</sub>).

## **Experimental Section**

### **Materials and methods**

All chemicals were purchased from commercial sources and used without any further purification: Cr(NO<sub>3</sub>)<sub>3</sub>·9H<sub>2</sub>O (98.5% Alfa Aesar), terephthalic acid (98 %, Sigma Aldrich), 2-aminoterephthalic acid (> 98 %, TCI Chemicals), 2-sulfoterephthalic acid monosodium salt (> 98 %, TCI Chemicals), Cytochrome c from bovine heart (≥ 95 %, Sigma-Aldrich). Thioanisole (> 99 % TCI Chemicals), 4-nitrothioanisole (99 %, ACROS Organics), 4-methylthioanisole (> 99 %, TCI Chemicals), and 4-methoxythioanisole (99 %, ACROS Organics).

## Synthesis of MOFs

MIL-101(Cr) was synthesized according to an already reported microwave-assisted hydrothermal synthesis.<sup>40</sup> MIL-101(Cr)-NH<sub>2</sub> was synthesized according to an already reported hydrothermal procedure.<sup>41</sup> For the synthesis of MIL-101(Cr)-SO<sub>3</sub>H, 400 mg of Cr(NO<sub>3</sub>)<sub>3</sub>·9H<sub>2</sub>O (1 mmol) and 840 mg of 2-sulfoterephthalic acid (3 mmol, BDC-SO<sub>3</sub>H) were added in a 15 mL Teflon reactor and dissolved in 5 mL of tetramethylammonium hydroxide (TMAOH) solution at 27 mM. The reaction mixture was heated under autogeneous pressure at 190 °C for 24 h. After cooling down to room temperature, the solid product was isolated by centrifugation and washed three times with H<sub>2</sub>O and three times with absolute ethanol. The resulting particles were kept in ethanolic suspension.

## Purification of Microperoxidase 8

MP8 was prepared and purified as described previously in the literature.<sup>42</sup> Briefly, 400 mg of Cyt c were mixed with 10.4 mg of pepsin and dissolved in 5 mL of H<sub>2</sub>O. The pH of the solution was adjusted to 2.6 with 1 M HCl. The mixture was incubated for 1 h at 37 °C. A second addition of 10.4 mg of pepsin was then performed and the pH was re-adjusted to 2.6. The incubation continued for 5 h and the main product of the reaction was microperoxidase 11 (MP11). The pepsin activity was stopped by raising the pH to 9, with the addition of a 38% v/v NH<sub>4</sub>HCO<sub>3</sub> solution. 8 mg of trypsin were then added for the digestion of MP11 to MP8 and the mixture was incubated at 37 °C overnight. MP8 was collected from the reaction mixture by gel filtration chromatography (biogel P6, 4 × 100 cm). The purified MP8 was lyophilized and stored at 4 °C. The concentration of the MP8 solution was calculated using the reported extinction coefficient,  $\epsilon_{396} = 1.57 \times 10^5 \text{ M}^{-1} \cdot \text{cm}^{-1}$ .<sup>42</sup>

### **Immobilization of MP8 into MIL-101(Cr)-X (X = H, NH<sub>2</sub>, SO<sub>3</sub>H)**

An aqueous solution of MP8 (1 mg/mL) was mixed with the respective MIL-101(Cr)-X particles, suspended in ethanol (5 mg/mL). The pH of the mixtures was adjusted to 5 for MIL-101(Cr) and MIL-101(Cr)-NH<sub>2</sub>, and to 3 for MIL-101(Cr)-SO<sub>3</sub>H. The mixtures were incubated at 37 °C and gently shaken for 48 h. The immobilized catalysts (MP8@MIL-101(Cr)-X) were washed several times with H<sub>2</sub>O to remove loosely bound enzyme molecules from the MOF surfaces and stored at 4 °C in aqueous suspensions. The MP8 loadings were evaluated by ICP-OES, through the quantification of Cr and Fe from the MOFs and the enzyme, respectively. Typically, a sample was heated at 100 °C overnight to evaporate the remaining solvent. Afterwards, 1 mL of HCl (37 %) was added and the sample was heated overnight (16 h) in a closed vial at 80 °C, for total mineralization. The sample was diluted to 40 mL with ultrapure H<sub>2</sub>O before the analysis.

### **Imidazole coordination studies**

1 μM catalyst (free MP8, MP8@MIL-101(Cr) and MP8@MIL-101(Cr)-SO<sub>3</sub>H) was incubated with increasing concentrations of imidazole (ImH) in phosphate buffer (0.01 M) at pH 7. The UV-visible spectrum of the sample was then recorded between 400 and 700 nm after each addition of ImH. Upon ImH addition, the initial maximum absorbance wavelength of MP8 ( $\lambda_{\max}$ = 396 nm) shifted progressively to  $\lambda_{\max}$ = 404 nm, due to the formation of the MP8(ImH) complex.<sup>43</sup>

### **Oxidation of ABTS by free MP8 and MP8@MIL-101(Cr)-X**

The catalytic activity of free MP8 and MP8@MIL-101-X was evaluated using 2,2'-azino-bis(3-ethylbenzothiazoline-6-sulphonic acid) (ABTS), which is catalytically

oxidized into ABTS<sup>•+</sup> radical cation in the presence of H<sub>2</sub>O<sub>2</sub>. The activity was measured by monitoring the increase in absorbance of ABTS<sup>•+</sup> at 420 nm ( $\epsilon_{420}=3.6 \times 10^4 \text{ M}^{-1}\cdot\text{cm}^{-1}$ ) as a function of time.<sup>44</sup> The reactions were typically performed with equal amount of MP8 (0.35  $\mu\text{M}$  either as free MP8 or immobilized MP8@MIL-101-X), 2 mM ABTS, 0.1-1.8 mM H<sub>2</sub>O<sub>2</sub> in citrate buffer (0.01 M) at pH 5 or in phosphate buffer (0.01 M) at pH 7 at RT, in a total volume of 3 mL. The total reaction time was fixed to 300 sec. The reaction rates were calculated by the slope of the absorbance (at 420 nm) over time for the first 20 sec of the reaction.

### **Recycling study of MP8@MIL-101(Cr)-NH<sub>2</sub>**

The recycling of MP8@MIL-101(Cr)-NH<sub>2</sub> was performed using 2.5 mg immobilized MP8@MIL-101(Cr)-NH<sub>2</sub> in 5 mL of phosphate buffer (0.01 M) at pH 7.4 at room temperature. 0.8 mM ABTS and 0.5 mM H<sub>2</sub>O<sub>2</sub> was added to the reaction mixture under stirring for 5 min. The mixture was then separated by centrifugation (14500 rpm, 20 min) and the supernatant was analyzed by UV-vis spectrometry to quantify the amount of oxidized ABTS. The recovered MP8@MIL-101(Cr)-NH<sub>2</sub> was dispersed in 5 mL of buffer solution and 0.5 mM H<sub>2</sub>O<sub>2</sub> was added under stirring for 5 min to further oxidized unreacted ABTS. The mixture was then separated by centrifugation (14500 rpm, 20 min) and the supernatant was analyzed by UV-vis spectrometry. The recovered MP8@MIL-101(Cr)-NH<sub>2</sub> was washed with 5 mL buffer solution, then centrifuged and the supernatant was analyzed by UV-vis spectrometry. The amount of oxidized ABTS was quantified by UV-Vis measurements of the three supernatants. The catalyst was then reused following the same procedure. The relative activity of the biocatalyst corresponds to the ratio of each cycle's activity over the activity of the first recycling cycle. The error bars

corresponds to the experimental error of each measurement.

### **Stability of MP8@MIL-101(Cr)-NH<sub>2</sub>**

The stability of MP8@MIL-101(Cr)-NH<sub>2</sub> under storage (4 °C, aqueous media) was evaluated based on their ability to catalyze the oxidation of ABTS. The reactions were performed with 0.35 μM immobilized MP8 (0.02 mg MP8@MIL-101(Cr)-NH<sub>2</sub>), 2 mM ABTS and 0.9 mM H<sub>2</sub>O<sub>2</sub> in phosphate buffer (0.01 M) at pH 7.4, at room temperature. The total reaction time was fixed to 5 min. The relative activity of the biocatalyst corresponds to the ratio of the day's activity over the activity of the first day. The error bars corresponds to the experimental error of each measurement.

### **Sulfoxidation reactions catalyzed by free MP8 and MP8@MIL-101(Cr)-X**

The reactions were performed with 1 mM of the respective thioanisole substrate (thioanisole, 4-nitrothioanisole, 4-methylthioanisole, and 4-methoxythioanisole), equal amount of MP8 (1 μM either as free MP8 or immobilized MP8@MIL-101-X), and 0.5 mM H<sub>2</sub>O<sub>2</sub> in a mixture 80:20 v/v phosphate buffer (0.01 M, pH 7):CH<sub>3</sub>CN, at RT, under stirring with a total volume of 0.5 mL. The total reaction time was fixed to 1 h. Acetophenone was added after 1 h as the internal standard for GC analysis. The sulfoxidized products were collected by extracting the organic phase with ethyl acetate and analyzed with GC. Retention times of respective sulfoxides: 7.4 min (thioanisole), 9.2 min (4-nitrothioanisole), 8.4 min (4-methylthioanisole) and 9.6 min (4-methoxythioanisole) and 4 min for acetophenone (internal standard).

## Characterizations

Powder X-ray diffraction was carried out with a Bruker D8 Advance diffractometer working on transmission mode and equipped with a focusing Göbel mirror producing  $\text{CuK}\alpha$  radiation ( $\lambda = 1.5418 \text{ \AA}$ ) and a LynxEye detector. Infrared spectra were collected with a ThermoScientific Nicolet 6700 FT-IR. Micro-Raman spectra were collected on a Horiba Jobin Yvon Labram HR 8500 (confocal) spectrometer, with an excitation wavelength of 488 nm and  $P = 1.175 \text{ mW}$ . Scanning electron microscopy (SEM) images were recorded on a JEOL JSM-7001F microscope, using gold-coated samples. TEM/STEM observations were made on a Titan Themis 200 microscope (FEI/ Thermo Fischer Scientific) equipped with a geometric aberration corrector on the probe. The microscope is also equipped with the "Super-X" systems for EDX analysis with a detection angle of 0.9 steradian. The observations were made at 200 kV with a probe current of about 45 pA and a half-angle of convergence of 17 mrad. HAADF-STEM images were acquired with a camera length of 110 mm (inner/outer collection angles are respectively 69 and 200 mrad). Dynamic light scattering (DLS)/ $\zeta$ -potential measurements were performed on a Malvern Instrument Zetasizer Nano ZS (**experimental details in SI**). Inductively coupled plasma optical emission spectroscopy (ICP-OES) was carried out with an Agilent 720 Series with axially-viewed plasma and with a Cr/Fe calibration curve of 50-30,000 ppb. Ultraviolet–visible (UV-vis) spectra were collected on a PerkinElmer LAMBDA 750 UV/Vis/NIR Spectrophotometer. Gas chromatography analyses were performed with a SHIMADZU GC-2014A, equipped with a Zebron ZB Semi Volatiles column (30 m  $\times$  0.25 mm  $\times$  0.25 mm).

## Results and Discussion

### Synthesis and characterization of MIL-101(Cr)-X (X = H, NH<sub>2</sub>, SO<sub>3</sub>H)

MIL-101(Cr) and the two functionalized analogues, MIL-101(Cr)-NH<sub>2</sub> and MIL-101(Cr)-SO<sub>3</sub>H were selected based on their difference in polarity, acidity and surface charge of particles. These physico-chemical properties of the MOFs may affect their interaction with MP8. MIL-101(Cr) and MIL-101(Cr)-NH<sub>2</sub> were synthesized following already reported protocols.<sup>40,41</sup> For MIL-101(Cr)-SO<sub>3</sub>H, a novel synthetic protocol was developed to avoid the use of toxic chemicals (e.g. Cr(VI) - CrO<sub>3</sub><sup>45</sup> or hydrofluoric acid<sup>46</sup>) and reduce the reaction time. The synthetic conditions were based on the protocol reported for the synthesis of MIL-101(Cr) by Yang *et al*, who employed tetramethylammonium hydroxide (TMAOH) as a base to increase the reaction pH to 6, improving the solubility of terephthalic acid and thus the sample's crystallinity.<sup>47</sup> The nature of the chromium precursor (Cr(NO<sub>3</sub>)<sub>3</sub>·9H<sub>2</sub>O) as well as the molar metal:ligand:TMAOH ratio were varied and found to be key parameters for the successful synthesis of MIL-101(Cr)-SO<sub>3</sub>H.

As indicated from the X-ray powder diffraction (XPRD) patterns in **Fig. 1**, the Bragg diffraction peaks of MIL-101(Cr)-X are in agreement with the calculated pattern of MIL-101(Cr). The main difference between the MIL-101(Cr)-X analogues concerns the crystallinity, which was lower for MIL-101(Cr)-NH<sub>2</sub> and higher for MIL-101(Cr)-SO<sub>3</sub>H and may partly result from the particles size. The broad peaks for MIL-101(Cr) and MIL-101(Cr)-NH<sub>2</sub> are indeed consistent with nanoscale particle size (~50 nm for MIL-101(Cr), ~ 70 nm MIL-101(Cr)-NH<sub>2</sub> and ~200 nm for MIL-101(Cr)-SO<sub>3</sub>H) as indicated

by SEM images in **Fig. S2**). The particles of these MOFs are in the nanoscale range, which favors the diffusion kinetics of reactants during the catalytic process.<sup>14,17</sup>

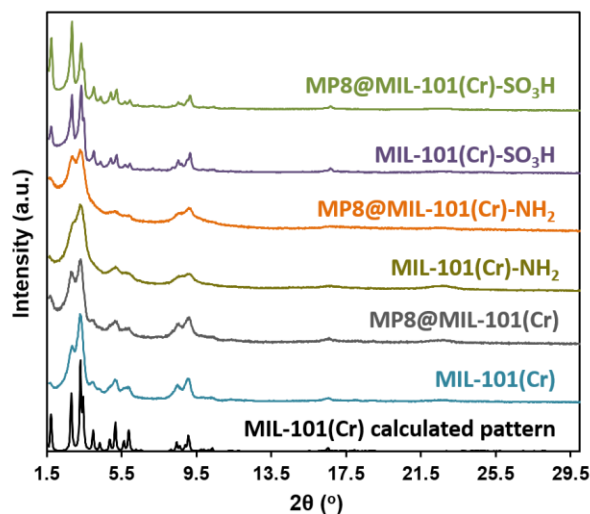


**Figure 1** PXRD patterns prior and after immobilization of MP8 within MIL-101(Cr), MIL-101(Cr)-NH<sub>2</sub>, MIL-101(Cr)-SO<sub>3</sub>H and the calculated pattern of MIL-101(Cr).

As a novel synthesis was used for MIL-101(Cr)-SO<sub>3</sub>H, it was further characterized by elemental analysis (C: 29.4 ± 0.3 % and S: 6.4 ± 0.1 %), indicating that 64 % of the ligands in the MOF framework contained the sulfonic acid groups. The incomplete substitution can be explained by the purity of the starting ligand (98%), since functionalized and non-modified ligands may not present the same reactivity. It may also result from a partial degradation of some sulfonic acid groups during the synthesis. The surface areas of the functionalized MOFs (nitrogen adsorption/desorption isotherms in **Fig. S3**) are lower (2417 and 2149 m<sup>2</sup>/g for MIL-101(Cr)-NH<sub>2</sub> and -SO<sub>3</sub>H, respectively) than the bare MOF (2951 m<sup>2</sup>/g), as a result of the presence of the pending functional groups reducing the pores volume.

## MP8@MIL-101(Cr)-X (X = H, NH<sub>2</sub>, SO<sub>3</sub>H): Synthesis and Characterizations

Prior to immobilization, in order to evaluate the possible electrostatic interactions between MP8 and the MOFs, the charge of MP8 and the MOF particles was measured by  $\zeta$ -potential as a function of pH (Fig. 2). MIL-101(Cr) and MIL-101(Cr)-NH<sub>2</sub> are positively charged under acidic conditions with a point of zero charge around 7. This value is higher than the one reported for most iron polycarboxylate MOFs (typically around 4-5),<sup>48</sup> suggesting that the particles charge is not solely driven by the carboxylate groups but also by the inorganic secondary units (protonation of water molecules and hydroxyls coordinated to the open metal sites).<sup>49</sup> The particle charge of MIL-101(Cr)-SO<sub>3</sub>H is negative over the whole pH range due to the presence of negatively charged SO<sub>3</sub><sup>-</sup> groups.

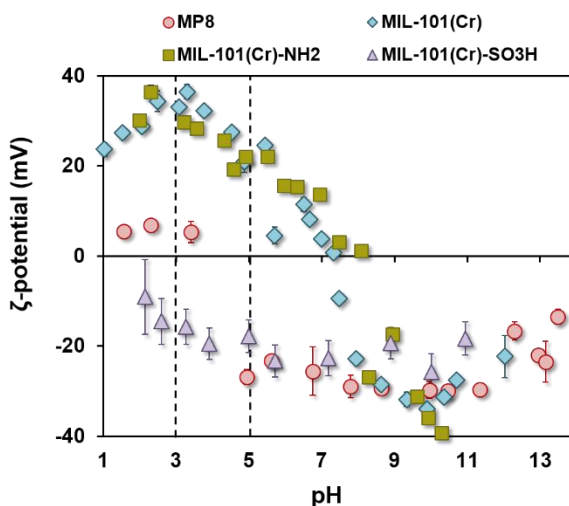


**Figure 2**  $\zeta$ -potential measurements of MP8 (circles), MIL-101(Cr) (diamonds), MIL-101(Cr)-NH<sub>2</sub> (squares) and MIL-101(Cr)-SO<sub>3</sub>H (triangles) as a function of pH. Errors bar are the standard deviation of three measurements.

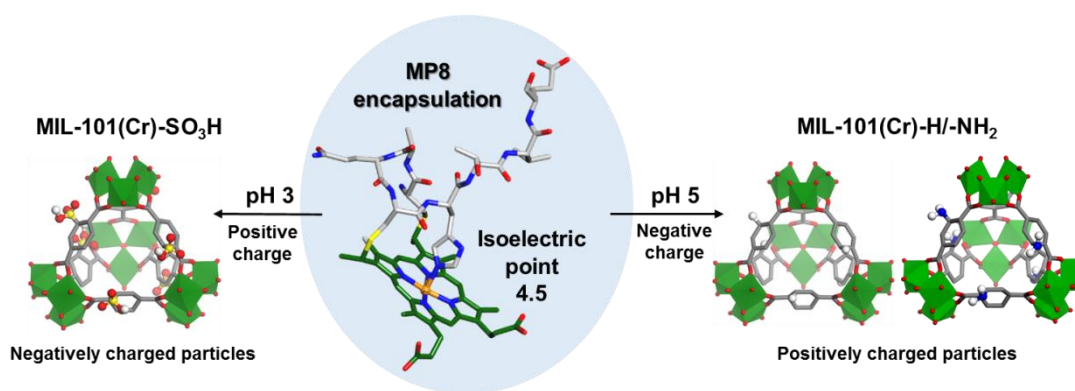
In the case of MP8, a positive charge was observed at  $\text{pH} \leq 4$ , mostly due to the protonation of the free carboxylic acid groups of the heme and of the proximal His18, in agreement with the  $\text{pK}_a = 4.4$  reported in the literature (**Fig. S4**).<sup>50</sup> Above this  $\text{pH}$ , MP8 showed a negative charge since the carboxylic acid groups of the enzyme and the water molecule coordinated to the sixth axial position of Fe(III) are deprotonated (**Fig. S4**).

The MP8 immobilization was performed by simply mixing MP8 with a suspension of MIL-101(Cr)-X at room temperature for 48 hours. Based on the  $\zeta$ -potential measurements, the  $\text{pH}$  value was fixed to 5, where the attractive electrostatic interactions between MP8 and MIL-101(Cr) or MIL-101(Cr)-NH<sub>2</sub> were optimal. The MP8 loading of the resulting MP8@MIL-101(Cr)-X materials was determined experimentally by inductively coupled plasma atomic emission spectroscopy (ICP-OES) based on the Fe/Cr ratio found in MP8 and MIL-101(Cr)-X. The MP8 loadings were also confirmed from the remaining MP8 amounts in the supernatants measured by UV-Vis spectroscopy. As seen in **Table 1** at  $\text{pH}$  5, MP8@MIL-101(Cr) showed a 5.0 % w/w loading of MP8, while a higher loading (8.1 % w/w) was found for MP8@MIL-101(Cr)-NH<sub>2</sub>. The encapsulation of MP8 in MP8@MIL-101(Cr)-SO<sub>3</sub>H at  $\text{pH}$  5 was not successful due to the repulsive coulombic interactions between MP8 and MIL-101(Cr)-SO<sub>3</sub>H, since they were both negatively charged at  $\text{pH}$  5. The immobilization was thus performed at  $\text{pH}$  3, where opposite charges between MP8 and MIL-101(Cr)-SO<sub>3</sub>H are observed (**Fig. 2 and Scheme 1**). The obtained MP8@MIL-101(Cr)-SO<sub>3</sub>H showed a MP8 loading of 7.2 % w/w, suggesting that coulombic interactions are an important driving force in the immobilization procedure.

**Table 1.** MP8 loading in MIL-101(Cr)-X determined by ICP-OES

Catalyst	MP8 loading (w/w %)
MP8@MIL-101(Cr)	5.0 ± 0.3
MP8@MIL-101(Cr)-NH <sub>2</sub>	8.1 ± 0.5
MP8@MIL-101(Cr)-SO <sub>3</sub> H (pH 3)	7.2 ± 0.1
MP8@MIL-101(Cr)-SO <sub>3</sub> H (pH 5)	-

As previously mentioned, the pores volumes of the functionalized MIL-101(Cr) analogues are lower than the bare MOF (**Fig. S3**), due to the presence of the functional pending groups. It was thus not expected that functionalized MOFs would lead to higher MP8 loadings. This may be due to specific interactions (H-bonding, additional electrostatic interactions etc...) between some -NH<sub>2</sub> /-NH<sub>3</sub><sup>+</sup> and -SO<sub>3</sub><sup>-</sup>/-SO<sub>3</sub>H groups of the functionalized MOFs and the carboxylic groups of the heme and amino-acid side chain of MP8. These results are in agreement with previous immobilization studies, in which the amino-functionalization of porous matrices resulted in higher enzyme loadings.<sup>24</sup>



**Scheme 1** Molecular structure of MP8, containing an Fe(III) porphyrin and the amino acid residues 14-21 of Cytochrome c (Structural data were obtained from the structure resolution of PDB·1OCD).<sup>51</sup> Schematic representation of the immobilization process within MIL-101(Cr) and MIL-101(Cr)-NH<sub>2</sub> at pH 5 and MIL-101(Cr)-SO<sub>3</sub>H at pH 3.

The MP8@MIL-101(Cr)-X were thoroughly characterized. As revealed from the PXRD patterns shown in **Fig. 1**, the crystalline structure of MIL-101(Cr)-X was preserved after the immobilization of MP8 within the MOFs. MP8@MIL-101(Cr), MP8@MIL-101(Cr)-NH<sub>2</sub> and MP8@MIL-101(Cr)-SO<sub>3</sub>H showed decreased N<sub>2</sub> uptake and specific surface area (1498, 398 and 612 m<sup>2</sup>/g, respectively) (**Fig. S3**), consistent with the presence of MP8 in their porosity. The greater decrease for MP8@MIL-101(Cr)-NH<sub>2</sub> and MP8@MIL-101(Cr)-SO<sub>3</sub>H (84 and 72 % of specific surface loss, respectively) compared to MP8@MIL-101(Cr) (49 %) is in agreement with higher MP8 loadings. The distribution of MP8 in the bio-hybrids was evaluated by STEM-XEDs mapping based on Cr, Fe, N and S contents and shown in **Fig. S5-7**. The Fe content was attributed to the presence of MP8 and was detected throughout the sample, suggesting an overall homogeneous distribution of MP8 in MP8@MIL-101(Cr)-X.

From the FT-IR spectra (**Fig. S8**), once immobilized in the MIL-101(Cr)-X particles, the characteristic amide I, amide II and amide III vibrations of MP8 (1652, 1540 and 1413 cm<sup>-1</sup>, respectively) superimpose with the carboxylate vibration bands ( $\nu(\text{CO})_{\text{as}} = 1628$ ,  $\nu(\text{CO})_{\text{s}} = 1394$  cm<sup>-1</sup>) of the MOFs, leading to a slight broadening of the bands in the 1620-1510 cm<sup>-1</sup> region for MP8@MIL-101(Cr)-X. Raman spectroscopy was employed in order to examine thoroughly the presence of MP8 molecules in the MOF particles and investigate possible interactions. **Fig. 3** shows the Raman spectra of free MP8, MIL-101(Cr)-X and MP8@MIL-101(Cr)-X and the detailed attributions are reported in **Table S1**. The spectra of MP8@MIL-101(Cr)-X (X= H, NH<sub>2</sub>, SO<sub>3</sub>H) showed the presence of characteristic vibration modes of both the MP8 and MIL-101(Cr)-X, which thus confirmed the immobilization of MP8 in all MOF particles.

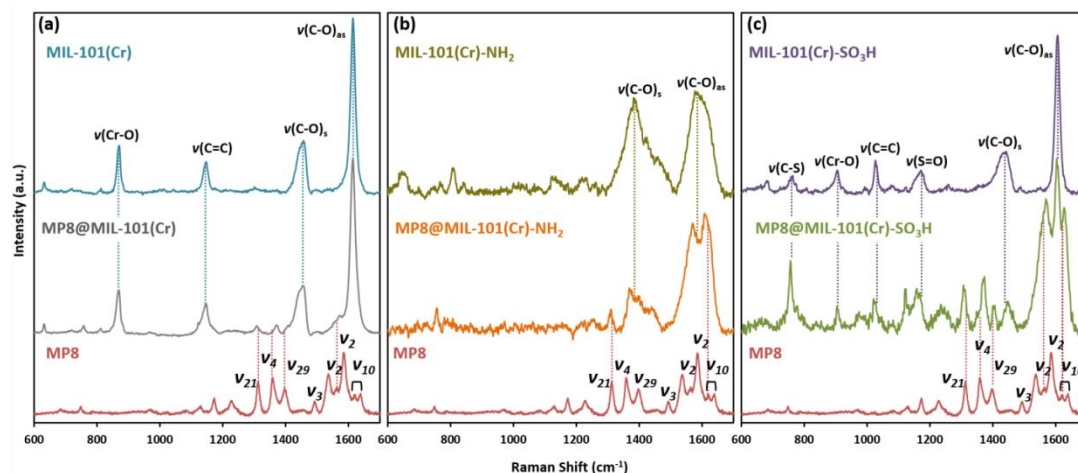


**Figure 3** Raman spectra of (a) free MP8 (red), MP8@MIL-101(Cr) (grey) and MIL-101(Cr) (blue); (b) free MP8 (red), MP8@MIL-101(Cr)-NH<sub>2</sub> (orange) and MIL-101(Cr)-NH<sub>2</sub> (brown); (c) free MP8 (red), MP8@MIL-101(Cr)-SO<sub>3</sub>H (green) and MIL-101(Cr)-SO<sub>3</sub>H (purple).

MIL-101(Cr), MIL-101(Cr)-NH<sub>2</sub>, and MIL-101(Cr)-SO<sub>3</sub>H exhibited vibrations, characteristic of the asymmetric and symmetric carboxylate stretching modes (1615/1453, 1580/1393 and 1607/1445 cm<sup>-1</sup>, respectively). Note that, due to the low crystallinity of MIL-101(Cr)-NH<sub>2</sub>, its vibration bands are broad and cannot all be clearly identified. The spectra of MIL-101(Cr) and MIL-101(Cr)-SO<sub>3</sub>H also displayed stretching modes of the ν(C=C) of the aromatic system (1154 cm<sup>-1</sup> and 1172 cm<sup>-1</sup>, respectively) and the symmetric stretching band ν(Cr-O) of the chromium trimers (869 and 900 cm<sup>-1</sup>, respectively).<sup>52</sup> In the case of MIL-101(Cr)-SO<sub>3</sub>H, two additional bands at 1100 cm<sup>-1</sup> and 763 cm<sup>-1</sup> can be assigned to the ν(S=O) and ν(C-S) modes of the sulfonic groups. The frequencies of the skeletal stretching modes of the heme in MP8 are located in the high-frequency region, 1300-1600 cm<sup>-1</sup>.<sup>43</sup> The bands related to the iron(III) coordination and spin state are ν<sub>10</sub>, ν<sub>3</sub>, and ν<sub>2</sub> and are summarized in **Table 2** and **S1** and are schematically represented in **Fig. S9**.

**Table 2.** High-frequency Raman modes ( $\text{cm}^{-1}$ ) of free and immobilized MP8

Catalyst	Hexacoordinated low-spin state			Pentacoordinated high-spin state			$\nu_4$
	$\nu_{10}$	$\nu_3$	$\nu_2$	$\nu_{10}$	$\nu_3$	$\nu_2$	
MP8	1639	-	1585	1620	1456	1565	1359 ( $\text{Fe}^{2+}$ )
MP8@MIL-101(Cr)	Overlap $\nu(\text{C-O})_{\text{as}}$	Overlap $\nu(\text{C-O})_{\text{s}}$	-	Overlap $\nu(\text{C-O})_{\text{as}}$	Overlap $\nu(\text{C-O})_{\text{s}}$	1572	1371 ( $\text{Fe}^{3+}$ )
MP8@MIL-101(Cr)- $\text{NH}_2$	-	-	Overlap $\nu(\text{C-O})_{\text{as}}$	1622	1451	Overlap $\nu(\text{C-O})_{\text{as}}$	-
MP8@MIL-101(Cr)- $\text{SO}_3\text{H}$	-	Overlap $\nu(\text{C-O})_{\text{s}}$	-	1629	Overlap $\nu(\text{C-O})_{\text{s}}$	1568	1371 ( $\text{Fe}^{3+}$ )

The vibration bands related to pentacoordinated high-spin iron (5C-HS) are at lower energy than the ones of the hexacoordinated low-spin iron (6C-LS) species (**Table 2**). In the spectrum of free MP8, these vibration bands are indicative of the presence of both 5C-HS and 6C-LS iron. The 5C-HS form corresponds to the monomeric form of MP8, whereas the 6C-LS form is attributed to intermolecular bonding between MP8 molecules due to the coordination of the terminal  $-\text{NH}_2$  of one MP8 molecule in the sixth axial position of the iron(III) atom of another molecule, trans to the imidazole moiety of His 18. This leads to the formation of aggregates.<sup>43,53</sup> Surprisingly, the oxidation state marker band,  $\nu_4$ , for free MP8 was observed at  $1359 \text{ cm}^{-1}$  characteristic of  $\text{Fe(II)}$  sites of MP8, instead of  $\sim 1370 \text{ cm}^{-1}$  for  $\text{Fe(III)}$  sites of MP8.<sup>54</sup> The reduction of  $\text{Fe}^{3+}$  center to  $\text{Fe}^{2+}$  in free MP8 was possibly due to the laser irradiation of the sample, as similar changes have been reported for heme containing enzymes.<sup>55</sup> Not all  $\nu_{10}$ ,  $\nu_3$ , and  $\nu_2$  modes were visible for MP8@MIL-101(Cr)-X due to overlapping with the MIL-101(Cr)-X modes, however, the visible modes ( $\nu_2$  for MP8@MIL-101(Cr),  $\nu_{10}$  and  $\nu_3$  for MP8@MIL-101(Cr)- $\text{NH}_2$ ,  $\nu_{10}$  and  $\nu_2$  for MP8@MIL-101(Cr)- $\text{SO}_3\text{H}$ , detailed in **Table 2**) are characteristic of iron 5C-HS species. It suggests that the immobilized MP8 molecules may mainly be under the monomeric form and thus their dispersion in the MOF frameworks avoided their

aggregation. Moreover, the  $\nu_4$  modes of MP8@MIL-101(Cr) and MP8@MIL-101(Cr)-SO<sub>3</sub>H indicated a Fe(III) site of MP8 (1371 cm<sup>-1</sup>), which was thus not reduced under the laser irradiation, suggesting a protection of MP8 by its encapsulation in the MOFs. Other characteristic modes of MP8 are  $\nu_{29}$  and  $\nu_{21}$  (1398 and 1313 cm<sup>-1</sup>), which were slightly shifted in the cases of MP8@MIL-101(Cr) (1405 and 1309 cm<sup>-1</sup>) and MP8@MIL-101(Cr)-SO<sub>3</sub>H (1404 and 1309 cm<sup>-1</sup>), indicative of interactions between MP8 molecules and the framework.<sup>56</sup>

The accessibility of the immobilized MP8 was then evaluated. The sixth axial position of Fe(III) in MP8 is occupied by a weakly bound water molecule, but it can easily be replaced by ligands with high binding affinity for the Fe(III) such as imidazole (ImH). ImH has been used in previous studies<sup>57</sup> to evaluate the accessibility of the Fe center of MP8 as its coordination to the Fe(III) results in a spectral evolution that can be easily monitored by UV-vis spectroscopy. The Soret band at 396 nm of free MP8 indeed gradually red shifts to 404 nm due to the formation of MP8(ImH) complexes. The accessibility of Fe(III) was evaluated for free MP8, MP8@MIL-101(Cr) and MP8@MIL-101(Cr)-SO<sub>3</sub>H. MP8@MIL-101(Cr)-NH<sub>2</sub> was not studied due to its poorer crystallinity. For all samples, a red shift was observed upon addition of imidazole, in agreement with the formation of MP8-ImH, thereby indicating that the Fe center of MP8 remained accessible upon immobilization within the MOFs (**Fig. S10**). The amounts of imidazole needed to reach the complete coordination of the MP8 Fe(III) center was 0.57, 3.7 and 7.83 mM for MP8, MP8@MIL-101(Cr) and MP8@MIL-101(Cr)-SO<sub>3</sub>H, respectively. The higher amounts of imidazole required for the immobilized MP8 suggests diffusional limitations, which is consistent with the inclusion of MP8 inside the mesoporosity of

MIL-101(Cr)-X. However, the imidazole concentration required for the complete MP8 complexation in MP8@MIL-101(Cr)-SO<sub>3</sub>H was twice higher than in the case of MP8@MIL-101(Cr), suggesting higher diffusion limitations of imidazole in MIL-101(Cr)-SO<sub>3</sub>H, possibly due to steric hindrance with the MOF substituents or interactions between imidazole molecules and the framework.

The combination of various advanced characterization techniques confirmed the successful immobilization of MP8 within MIL-101(Cr)-X as well as the preservation of the accessibility to its active site.

#### **Evaluation of the catalytic activity of MP8@MIL-101-X (X = H, NH<sub>2</sub>, SO<sub>3</sub>H)**

The catalytic activity of free and immobilized MP8 molecules with a similar MP8 content was evaluated using a typical peroxidase reaction: the oxidation of the chromogenic substrate ABTS into ABTS<sup>++</sup> ( $\lambda_{\text{max}} = 420 \text{ nm}$ ) in the presence of H<sub>2</sub>O<sub>2</sub>. No catalytic activity was detected for the three MOFs. **Fig. 4** shows the amounts of ABTS<sup>++</sup> formed after 300 sec and the initial reaction rates, with increasing concentrations of H<sub>2</sub>O<sub>2</sub> at pH 7 in the presence of equal amount of MP8 (0.35  $\mu\text{M}$  MP8 free or immobilized). Free MP8 oxidized faster the ABTS and resulted in higher concentrations of oxidized substrate compared to the immobilized enzymes (kinetics of the catalytic reactions in **Fig. S11**). The amounts of ABTS<sup>++</sup> as well as the rates of oxidation were similar for MP8@MIL-101(Cr) and MP8@MIL-101(Cr)-NH<sub>2</sub>, indicating that the intrinsic catalytic activity of MP8 is identical once immobilized in MIL-101(Cr) or in MIL-101(Cr)-NH<sub>2</sub>. On the contrary, the catalytic activity of MP8@MIL-101(Cr)-SO<sub>3</sub>H was low as shown by the moderate amounts of ABTS<sup>++</sup> converted and the almost negligible reaction rates. This could be due to the acidic conditions (pH 3), necessary for the MP8 immobilization in

MIL-101(Cr)-SO<sub>3</sub>H and the acidic environment within the MOFs pores. The negative  $\zeta$ -potential of MIL-101(Cr)-SO<sub>3</sub>H, indicates the presence of sulfonate groups with most likely free protons within the cavities. Under acidic conditions, free MP8 can be deactivated as a result of the cleavage of Fe(III)-His bond.<sup>20</sup> The same process may be occurring for MP8 immobilized in MIL-101(Cr)-SO<sub>3</sub>H, inducing a loss of catalytic activity.

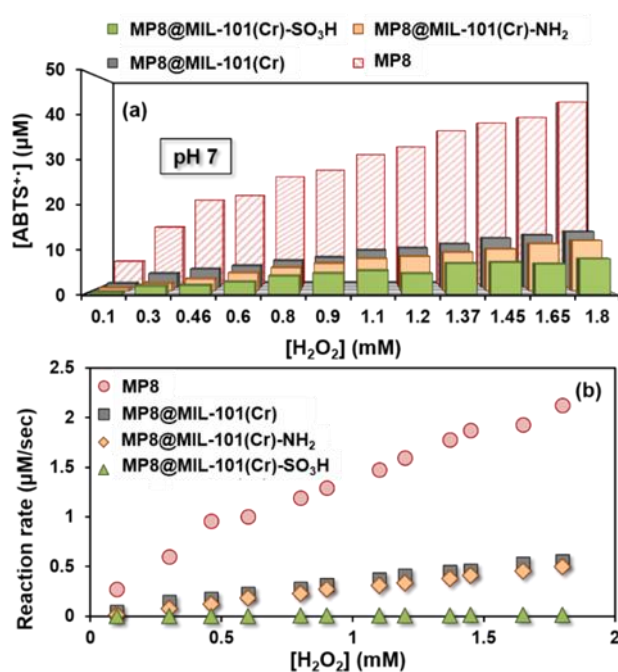


**Figure 4** (a) ABTS<sup>•+</sup> concentration and (b) initial reaction rates of the oxidation of ABTS in the presence of increasing concentrations of H<sub>2</sub>O<sub>2</sub> (0.1-1.8 mM) for equal amount of MP8 (0.35 μM either as free MP8 or immobilized MP8@MIL-101-X) in phosphate buffer at pH 7 for 300 sec of reaction. Errors bars are the standard deviation of three measurements.

In a previous work,<sup>22</sup> it has been demonstrated that the MOF framework can protect MP8 molecules under acidic conditions (pH 5) as a result of a confined micro-environment in

the pores that limits the protonation of the axial His18. The protective role of the framework was also examined for MIL-101(Cr)-NH<sub>2</sub>. Note that MIL-101(Cr)-SO<sub>3</sub>H was not studied due to its poor performances at pH 7. **Fig. 5** displays ABTS<sup>+</sup> amounts after 300 sec and the initial reactions rate of oxidation with increasing concentrations of H<sub>2</sub>O<sub>2</sub>, at pH 5 (kinetics of the catalytic reactions in **Fig. S12**). MIL-101(Cr) and MIL-101(Cr)-NH<sub>2</sub> revealed the same catalytic activity at similar MP8 content and both immobilized enzymes could catalyse the oxidation of higher amounts of ABTS with faster reaction rates than the free MP8, showing the protective role of the MOF framework toward acidic conditions.

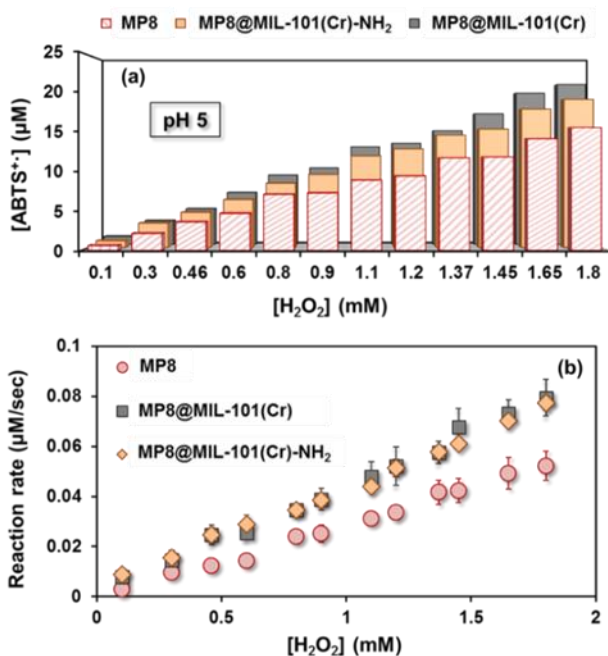


**Figure 5** (a) ABTS<sup>+</sup> concentration and (b) initial reaction rates of the oxidation of ABTS in the presence of increasing concentration of H<sub>2</sub>O<sub>2</sub> (0.1-1.8 mM) by equal amount of MP8 (0.35 µM either as free MP8 or immobilized MP8@MIL-101-X) in citrate buffer at pH 5 for 300 sec of reaction. Errors bars are the standard deviation of three measurements.

Since the reaction kinetics were slower for the MP8@MIL-101(Cr)-X, the oxidation of ABTS was also assessed for longer reaction times (1 hour). **Fig. 6a** illustrated the ABTS<sup>++</sup> amounts formed after 1 hour and **Fig S13a** the reaction kinetics for equal amount of free and immobilized MP8, with 0.9 mM H<sub>2</sub>O<sub>2</sub> and at pH 7. As observed, even though free MP8 led to a maximum ABTS<sup>++</sup> amount (35 μM) in less than 10 min, MP8@MIL-101(Cr) and MP8@MIL-101(Cr)-NH<sub>2</sub> were able to catalyse the oxidation of higher amounts of ABTS in 1 h (48 μM). Furthermore, for free MP8, the absorbance of ABTS<sup>++</sup> decreased with time as a result of its over oxidation (**Fig. S13a**).<sup>58</sup> Neither MP8@MIL-101(Cr) nor MP8@MIL-101(Cr)-NH<sub>2</sub> showed this effect, probably due to the stabilization of ABTS<sup>++</sup> by the MOFs framework, as previously reported.<sup>22,59</sup>

The catalytic activity was also evaluated with equivalent amounts of the heterogeneous biohybrid materials. When 2.6 mg of MP8@MIL-101(Cr) or MP8@MIL-101(Cr)-NH<sub>2</sub> were used, MP8@MIL-101(Cr)-NH<sub>2</sub> resulted in higher ABTS<sup>++</sup> amount (52 μM after 20 min), compared to MP8@MIL-101(Cr) (36 μM after 20 min) (**Fig 6b** and **Fig S13b**). The higher MP8 loading capacity of MIL-101(Cr)-NH<sub>2</sub> provides an enhanced catalytic activity to the heterogeneous biocatalyst.

The PXRD patterns of MP8@MIL-101(Cr) and MP8@MIL-101(Cr)-NH<sub>2</sub> were recorded after catalysis (**Fig S14**). No significant differences were observed in comparison to their PXRD patterns before catalysis, suggesting their crystalline structure is preserved and stable after catalysis.

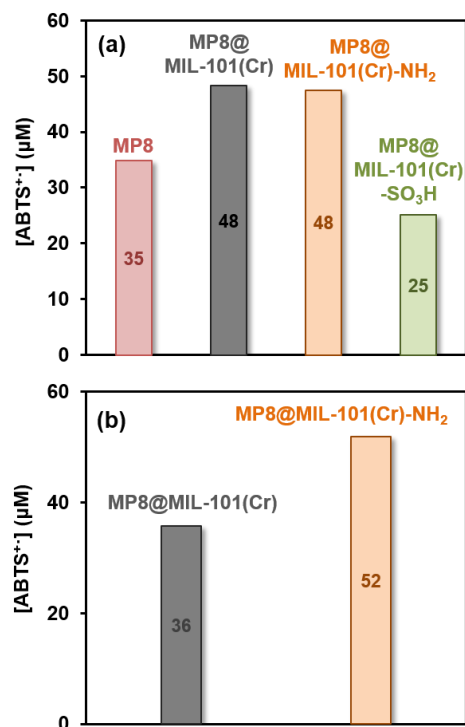


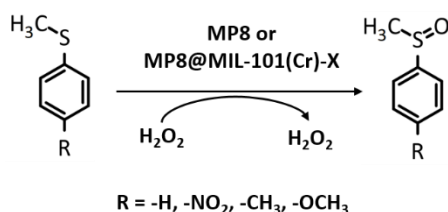
**Figure 6 (a)** ABTS<sup>+</sup> concentration with equal amount of MP8 (0.35 µM either as free MP8 or immobilized MP8@MIL-101-X), 0.9 mM H<sub>2</sub>O<sub>2</sub>, 2mM ABTS in phosphate buffer, pH 7 for 1 h reaction time and **(b)** ABTS<sup>+</sup> concentration with 0.3 mM H<sub>2</sub>O<sub>2</sub>, 0.7 mM ABTS, 2.6 mg MP8@MIL-101(Cr) or MP8@MIL-101(Cr)-NH<sub>2</sub> (equal amount of heterogeneous biocatalysts) for 20 min reaction time.

The catalytic activity of MP8@MIL-101(Cr) for the oxidation of ABTS by H<sub>2</sub>O<sub>2</sub> had previously been demonstrated to be relatively stable over 5 consecutive catalytic cycles.<sup>22</sup> Moreover this material exhibited a good catalytic activity and chemical stability under storage over one month at 4°C.<sup>22</sup> The recycling and long term stability of MP8@MIL-101(Cr)-NH<sub>2</sub> were evaluated and shown in **Figure S15**. The biocatalyst could be recycled over 5 consecutive catalytic cycles (**Fig. S15a**). The catalytic activity decreased by 10 % after the first cycle and then remained constant over the following catalytic tests,

indicating a good stability of the biocatalyst. The PXRD pattern of MP8@MIL-101(Cr)-NH<sub>2</sub> after 5 catalytic cycles (**Fig. S14**) shows the preservation of the crystalline structure of the framework during the recycling test. The catalytic activity of the material, stored at 4 °C, was also assessed over 3 weeks (**Fig. S15b**) and was found to be stable over time.

### Catalytic sulfoxidation of thioanisole derivatives to sulfoxides

The ability of free and immobilized MP8 to catalyze the sulfoxidation of different para-substituted thioanisole derivatives, in presence of H<sub>2</sub>O<sub>2</sub> was investigated (**Scheme 2**) and the produced sulfoxides were quantified by gas chromatography. The reactivity of para-substituted thioanisole derivatives for the electrophilic oxygen transfer reaction is known to increase with electron donating group (EDG) as substituents, with the order 4-methoxythioanisole (strong activator) > 4-methylthioanisole (weak activator) > thioanisole > 4-nitrothioanisole (strong deactivator).<sup>60</sup>



**Scheme 2** Oxidation of thioanisole derivatives catalyzed by free MP8 or MP8@MIL-101(Cr)-X, in presence of H<sub>2</sub>O<sub>2</sub>.

No product was detected in the absence of MP8 in a medium containing thioanisole derivatives, 1 mM H<sub>2</sub>O<sub>2</sub> and 0.5 mM MIL-101(Cr)-X. As seen in **Fig. 7** and **Table S2**, the immobilized MP8@MIL-101(Cr)-X catalyzed the selective oxidation of thioanisole derivatives to the respective sulfoxides. MP8@MIL-101(Cr)-X resulted in lower conversion to sulfoxides compared to the free enzyme due to diffusion limitation, as

previously explained. The catalytic activity of the bio-catalysts follows the order  $\text{MP8} > \text{MP8@MIL-101(Cr)} / \text{MP8@MIL-101(Cr)-NH}_2 > \text{MP8@MIL-101(Cr)-SO}_3\text{H}$  in agreement with the catalytic activity observed with the ABTS oxidation reactions. The most efficient conversion was achieved with the 4-methoxythioanisole derivative, bearing a strong EDG that may activate the electrophilic oxygen transfer reaction as previously shown.<sup>61</sup> The 4-methylthioanisole and thioanisole derivatives were also successfully converted. The sulfoxidation of 4-nitrothioanisole was very limited compared to the other thioanisole derivatives, which may be due to the strong electron withdrawing effect of the  $\text{NO}_2$  group (EWG). The impact of  $-\text{OCH}_3$  group (EDG) on the conversion of the thioanisole derivatives followed the same trend for free MP8 (+ 372 % increase), and MP8 immobilized within MIL-101(Cr)-X (+ 177 % and + 151 % increase for MIL-101(Cr) and MIL-101(Cr)- $\text{NH}_2$ , respectively).

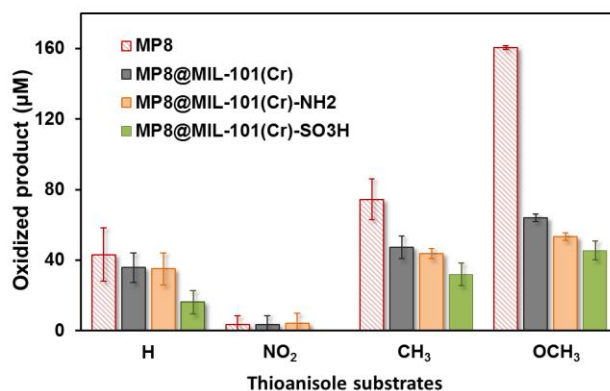


**Figure 7** Sulfoxidized amounts of 1 mM thioanisole derivatives with 0.5 mM  $\text{H}_2\text{O}_2$  by equal amount of MP8 (0.35  $\mu\text{M}$  either as free MP8 or immobilized  $\text{MP8@MIL-101-X}$ ), in 80:20 phosphate buffer (pH 7): $\text{CH}_3\text{CN}$  for 1 h of reaction.

## CONCLUSIONS

In conclusion, MIL-101(Cr) bearing different functionalized groups (-NH<sub>2</sub> and -SO<sub>3</sub>H) were used for the immobilization of microperoxidase 8 (MP8). The MP8@MIL-101(Cr)-X materials were characterized with a combination of characterisation techniques (PXRD, UV-Vis, IR and Raman Spectroscopies, N<sub>2</sub> sorption, ICP-OES), highlighting several important features. The crystalline structures of the MOFs were preserved after MP8 immobilization. The electrostatic interactions between the MP8 molecules and the MOF matrix were found to be a key parameter for a successful immobilization. Moreover, the presence of functional groups resulted in the immobilization of higher amounts of MP8 compared to those obtained with the bare MIL-101(Cr). This may be attributed to specific interactions between the MP8 molecules and the functionalized groups, as shown by Raman spectroscopy *via* shifts in the characteristic bands of MP8. Raman Spectroscopy was found to be a powerful tool to probe immobilized enzyme structure, as it also revealed that the immobilized MP8 molecules were dispersed in the MIL-101(Cr)-X matrices as monomers without aggregation. The catalytic activity toward a typical substrate (ABTS) was found to be very low for MP8@MIL-101(Cr)-SO<sub>3</sub>H. The acidic conditions for the encapsulation and the acidic environment of the MOF matrix may have caused the deprotonation of the histidine residue in MP8, which is detrimental for its catalytic activity. Similar catalytic activity was obtained for MP8@MIL-101(Cr) and MP8@MIL-101(Cr)-NH<sub>2</sub> at identical MP8 contents. In agreement with the already reported protective nature of MP8@MIL-101(Cr), MP8@MIL-101(Cr)-NH<sub>2</sub> could efficiently enhance MP8 catalytic activity under acidic conditions. Importantly, MIL-101(Cr)-NH<sub>2</sub> immobilized higher amounts of enzyme and thus the catalytic activity of

MP8@MIL-101(Cr)-NH<sub>2</sub> per material mass was found to be higher than for MP8@MIL-101(Cr). The presence of pending amino groups in the MOF could thus be a way to favour enzyme immobilization and the catalytic activity of other MOF-enzyme materials. MP8@MIL-101(Cr) and MP8@MIL-101(Cr)-NH<sub>2</sub> were also successfully used for the selective oxidation of thioanisole derivatives into sulfoxides. Similarly to free MP8, the immobilized enzymes were more reactive when sulfides bearing EDG groups were used.

## **ASSOCIATED CONTENT**

**Supporting Information** ζ-potential measurements, characterization of materials and catalytic studies. This material is available free of charge via the Internet at <http://pubs.acs.org>.

## **AUTHOR INFORMATION**

### **Corresponding Authors**

\*Clémence Sicard : E-mail: [clemence.sicard@uvsq.fr](mailto:clemence.sicard@uvsq.fr), [ORCID 0000-0002-3312-9025](https://orcid.org/0000-0002-3312-9025)

\* Remy Ricoux: E-mail: [remy.ricoux@u-psud.fr](mailto:remy.ricoux@u-psud.fr); [ORCID: 0000-0002-3464-7895](https://orcid.org/0000-0002-3464-7895)

### **Funding Sources**

This work was supported by the ANR-11-LABEX-0039 (LabEx charm<sub>3</sub>at).

### **Notes**

The authors declare no conflicts of interest.

## **ACKNOWLEDGMENT**

We thank Dr. M. Benzaqui and Dr. C. Livage for the SEM experiments, F. Bourdreux for the ICP-OES measurements, Dr. S. Devautour-Vinot and Magalie Lefeuvre, (Laboratoire

de Mesures Physiques, Université Montpellier) for the elemental analysis and Dr. A. Tissot for the nitrogen sorption measurements and fruitful discussions.

## REFERENCES

- (1) Velde, F. van de; Rantwijk, F. van; Sheldon, R. A. Improving the Catalytic Performance of Peroxidases in Organic Synthesis. *Trends Biotechnol.* **2001**, *19*, 73–80.
- (2) Ferrer, M. L.; Levy, D.; Gomez-Lor, B.; Iglesias, M. High Operational Stability in Peroxidase-Catalyzed Non-Aqueous Sulfoxidations by Encapsulation within Sol–Gel Glasses. *J. Mol. Catal. B Enzym.* **2004**, *27*, 107–111.
- (3) Šulek, F.; Fernández, D. P.; Knez, Ž.; Habulin, M.; Sheldon, R. A. Immobilization of Horseradish Peroxidase as Crosslinked Enzyme Aggregates (CLEAs). *Process Biochem.* **2011**, *46*, 765–769.
- (4) van de Velde, F.; Lourenço, N. D.; Bakker, M.; van Rantwijk, F.; Sheldon, R. A. Improved Operational Stability of Peroxidases by Coimmobilization with Glucose Oxidase. *Biotechnol. Bioeng.* **2000**, *69*, 286–291.
- (5) Hwang, E. T.; Gu, M. B. Enzyme Stabilization by Nano/Microsized Hybrid Materials: Enzyme Stabilization by Nano/Microsized Hybrid Materials. *Eng. Life Sci.* **2013**, *13*, 49–61.
- (6) Mousty, C.; Prevot, V. Hybrid and Biohybrid Layered Double Hydroxides for Electrochemical Analysis. *Anal. Bioanal. Chem.* **2013**, *405*, 3513–3523.
- (7) Lian, X.; Fang, Y.; Joseph, E.; Wang, Q.; Li, J.; Banerjee, S.; Lollar, C.; Wang, X.; Zhou, H.-C. Enzyme–MOF (Metal–Organic Framework) Composites. *Chem. Soc. Rev.* **2017**, *46*, 3386–3401.

- (8) Doonan, C.; Riccò, R.; Liang, K.; Bradshaw, D.; Falcaro, P. Metal–Organic Frameworks at the Biointerface: Synthetic Strategies and Applications. *Acc. Chem. Res.* **2017**, *50*, 1423–1432.
- (9) Majewski, M. B.; Howarth, A. J.; Li, P.; Wasielewski, M. R.; Hupp, J. T.; Farha, O. K. Enzyme Encapsulation in Metal–Organic Frameworks for Applications in Catalysis. *CrystEngComm* **2017**, *19*, 4082–4091.
- (10) Gkaniatsou, E.; Sicard, C.; Ricoux, R.; Mahy, J.-P.; Steunou, N.; Serre, C. Metal–Organic Frameworks: A Novel Host Platform for Enzymatic Catalysis and Detection. *Mater. Horiz.* **2017**, *4*, 55–63.
- (11) Patra, S.; Hidalgo Crespo, T.; Permyakova, A.; Sicard, C.; Serre, C.; Chaussé, A.; Steunou, N.; Legrand, L. Design of Metal Organic Framework–Enzyme Based Bioelectrodes as a Novel and Highly Sensitive Biosensing Platform. *J Mater Chem B* **2015**, *3*, 8983–8992.
- (12) Liang, K.; Ricco, R.; Doherty, C. M.; Styles, M. J.; Bell, S.; Kirby, N.; Mudie, S.; Haylock, D.; Hill, A. J.; Doonan, C. J.; Falcaro, P. Biomimetic Mineralization of Metal-Organic Frameworks as Protective Coatings for Biomacromolecules. *Nat. Commun.* **2015**, *6*, 7240.
- (13) Lykourinou, V.; Chen, Y.; Wang, X.-S.; Meng, L.; Hoang, T.; Ming, L.-J.; Musselman, R. L.; Ma, S. Immobilization of MP-11 into a Mesoporous Metal–Organic Framework, MP-11@mesoMOF: A New Platform for Enzymatic Catalysis. *J. Am. Chem. Soc.* **2011**, *133*, 10382–10385.
- (14) Lian, X.; Erazo-Oliveras, A.; Pellois, J.-P.; Zhou, H.-C. High Efficiency and Long-Term Intracellular Activity of an Enzymatic Nanofactory Based on Metal-Organic

- Frameworks. *Nat. Commun.* **2017**, *8*, 2075.
- (15) Li, P.; Chen, Q.; Wang, T. C.; Vermeulen, N. A.; Mehdi, B. L.; Dohnalkova, A.; Browning, N. D.; Shen, D.; Anderson, R.; Gómez-Gualdrón, D. A.; Cetin, F. M.; Jagiello, J.; Asiri, A. M.; Stoddart, J. F.; Farha, O. K. Hierarchically Engineered Mesoporous Metal-Organic Frameworks toward Cell-Free Immobilized Enzyme Systems. *Chem* **2018**, *4*, 1022–1034.
- (16) Li, P.; Modica, J. A.; Howarth, A. J.; Vargas L., E.; Moghadam, P. Z.; Snurr, R. Q.; Mrksich, M.; Hupp, J. T.; Farha, O. K. Toward Design Rules for Enzyme Immobilization in Hierarchical Mesoporous Metal-Organic Frameworks. *Chem* **2016**, *1*, 154–169.
- (17) Li, P.; Moon, S.-Y.; Guelta, M. A.; Lin, L.; Gómez-Gualdrón, D. A.; Snurr, R. Q.; Harvey, S. P.; Hupp, J. T.; Farha, O. K. Nanosizing a Metal–Organic Framework Enzyme Carrier for Accelerating Nerve Agent Hydrolysis. *ACS Nano* **2016**, *10*, 9174–9182.
- (18) Liang, W.; Xu, H.; Carraro, F.; Maddigan, N. K.; Li, Q.; Bell, S. G.; Huang, D. M.; Tarzia, A.; Solomon, M. B.; Amenitsch, H.; Vaccari, L.; Sumbly, C. J.; Falcaro, P.; Doonan, C. J. Enhanced Activity of Enzymes Encapsulated in Hydrophilic Metal–Organic Frameworks. *J. Am. Chem. Soc.* **2019**, *141*, 2348–2355.
- (19) Ricoux, R.; Korri-Youssoufi, H.; Mahy, J. P. Microperoxidase 8 as a Powerful Tool for Biological Applications. *J. Biol. Sci.* **2005**, *5*, 44–49.
- (20) Marques, H. M. Insights into Porphyrin Chemistry Provided by the Microperoxidases, the Haempeptides Derived from Cytochrome *c*. *Dalton Trans.* **2007**, *39*, 4371–438

- (21) Gkaniatsou, E.; Serre, C.; Mahy, J.-P.; Steunou, N.; Ricoux, R.; Sicard, C. Enhancing Microperoxidase Activity and Selectivity: Immobilization in Metal-Organic Frameworks. *J. Porphy. Phthalocyanines* **2019**, *23*, 1–11.
- (22) Gkaniatsou, E.; Sicard, C.; Ricoux, R.; Benahmed, L.; Bourdreux, F.; Zhang, Q.; Serre, C.; Mahy, J.-P.; Steunou, N. Enzyme Encapsulation in Mesoporous Metal-Organic Frameworks for Selective Biodegradation of Harmful Dye Molecules. *Angew. Chem. Int. Ed.* **2018**, *57*, 1–7.
- (23) Deng, H.; Grunder, S.; Cordova, K. E.; Valente, C.; Furukawa, H.; Hmadeh, M.; Gandara, F.; Whalley, A. C.; Liu, Z.; Asahina, S.; Kazumori, H.; O’Keeffe, M.; Terasaki, O.; Stoddart, J. F.; Yaghi, O. M. Large-Pore Apertures in a Series of Metal-Organic Frameworks. *Science* **2012**, *336*, 1018–1023.
- (24) Hartono, S. B.; Qiao, S. Z.; Liu, J.; Jack, K.; Ladewig, B. P.; Hao, Z.; Lu, G. Q. M. Functionalized Mesoporous Silica with Very Large Pores for Cellulase Immobilization. *J. Phys. Chem. C* **2010**, *114*, 8353–8362.
- (25) Navarro-Sánchez, J.; Imora-Barrios, N.; Lerma-Berlanga, B.; Ruiz-Pernía, J. J.; Lórenz-Fonfría, V. A.; Tuñón, I.; Martí-Gastaldo, C. Translocation of Enzymes into a Mesoporous MOF for Enhanced Catalytic Activity Under Extreme Conditions. *Chem Sci* **2019**, *10*, 4082–4088.
- (26) Lian, X.; Chen, Y.-P.; Liu, T.-F.; Zhou, H.-C. Coupling Two Enzymes into a Tandem Nanoreactor Utilizing a Hierarchically Structured MOF. *Chem. Sci.* **2016**, *7*, 6969–6973.
- (27) Li, P.; Moon, S.-Y.; Guelta, M. A.; Harvey, S. P.; Hupp, J. T.; Farha, O. K. Encapsulation of a Nerve Agent Detoxifying Enzyme by a Mesoporous Zirconium

- Metal–Organic Framework Engenders Thermal and Long-Term Stability. *J. Am. Chem. Soc.* **2016**, *138*, 8052–8055.
- (28) Lian, X.; Huang, Y.; Zhu, Y.; Fang, Y.; Zhao, R.; Joseph, E.; Li, J.; Pellois, J.-P.; Zhou, H.-C. Enzyme-MOF Nanoreactor Activates Nontoxic Paracetamol for Cancer Therapy. *Angew. Chem. Int. Ed.* **2018**, *57*, 5725–5730.
- (29) Pires, S. M. G.; Simões, M. M. Q.; Santos, I. C. M. S.; Rebelo, S. L. H.; Paz, F. A. A.; Neves, M. G. P. M. S.; Cavaleiro, J. A. S. Oxidation of Organosulfur Compounds Using an Iron(III) Porphyrin Complex: An Environmentally Safe and Efficient Approach. *Appl. Catal. B Environ.* **2014**, *160–161*, 80–88.
- (30) Sharma, V. K.; Luther, G. W.; Millero, F. J. Mechanisms of Oxidation of Organosulfur Compounds by Ferrate(VI). *Chemosphere* **2011**, *82*, 1083–1089.
- (31) Holland, H. L. Chiral Sulfoxidation by Biotransformation of Organic Sulfides. *Chem. Rev.* **1988**, *88*, 473–485.
- (32) Carreno, M. C. Applications of Sulfoxides to Asymmetric Synthesis of Biologically Active Compounds. *Chem. Rev.* **1995**, *95*, 1717–1760.
- (33) Fernández, I.; Khair, N. Recent Developments in the Synthesis and Utilization of Chiral Sulfoxides. *Chem. Rev.* **2003**, *103*, 3651–3706.
- (34) Wojaczyńska, E.; Wojaczyński, J. Enantioselective Synthesis of Sulfoxides: 2000–2009. *Chem. Rev.* **2010**, *110*, 4303–4356.
- (35) Wang, R.; Zhang, G.; Zhao, H. Polyoxometalate as Effective Catalyst for the Deep Desulfurization of Diesel Oil. *Catal. Today* **2010**, *149*, 117–121.
- (36) Khorshidifard, M.; Rudbari, H. A.; Askari, B.; Sahihi, M.; Farsani, M. R.; Jalilian, F.; Bruno, G. Cobalt(II), Copper(II), Zinc(II) and Palladium(II) Schiff Base

Complexes: Synthesis, Characterization and Catalytic Performance in Selective Oxidation of Sulfides Using Hydrogen Peroxide under Solvent-Free Conditions. *Polyhedron* **2015**, *95*, 1–13.

- (37) Lang, X.; Leow, W. R.; Zhao, J.; Chen, X. Synergistic Photocatalytic Aerobic Oxidation of Sulfides and Amines on TiO<sub>2</sub> under Visible-Light Irradiation. *Chem. Sci.* **2015**, *6*, 1075–1082.
- (38) Dai, L.; Klivanov, A. M. Peroxidase-Catalyzed Asymmetric Sulfoxidation in Organic Solvents versus in Water. *Biotechnol. Bioeng.* **2000**, *70*, 353–357.
- (39) van de Velde, F.; Arends, I. W. C. E.; Sheldon, R. A. Biocatalytic and Biomimetic Oxidations with Vanadium. *J. Inorg. Biochem.* **2000**, *80*, 81–89.
- (40) Demessence, A.; Horcajada, P.; Serre, C.; Boissière, C.; Grosso, D.; Sanchez, C.; Férey, G. Elaboration and Properties of Hierarchically Structured Optical Thin Films of MIL-101(Cr). *Chem. Commun.* **2009**, *46*, 7149–7151.
- (41) Jiang, D.; Keenan, L. L.; Burrows, A. D.; Edler, K. J. Synthesis and Post-Synthetic Modification of MIL-101(Cr)-NH<sub>2</sub> via a Tandem Diazotisation Process. *Chem. Commun.* **2012**, *48*, 12025–12124.
- (42) Aron, J.; Baldwin, D. A.; Marques, H. M.; Pratt, J. M.; Adams, P. A. Hemes and Hemoproteins: 1: Preparation and Analysis of the Heme-Containing Octapeptide (Microperoxidase-8) and Identification of the Monomeric Form in Aqueous Solution. *J. Inorg. Biochem.* **1986**, *27*, 227–243.
- (43) Othman, S.; Le Lirzin, A.; Desbois, A. Resonance Raman Investigation of Imidazole and Imidazolate Complexes of Microperoxidase: Characterization of the Bis (Histidine) Axial Ligation in c-Type Cytochromes. *Biochemistry* **1994**, *33*,

15437–15448.

- (44) Kenzom, T.; Srivastava, P.; Mishra, S. Structural Insights into 2,2'-Azino-Bis(3-Ethylbenzothiazoline-6-Sulfonic Acid) (ABTS)-Mediated Degradation of Reactive Blue 21 by Engineered *Cyathus Bulleri* Laccase and Characterization of Degradation Products. *Appl. Environ. Microbiol.* **2014**, *80*, 7484–7495.
- (45) Akiyama, G.; Matsuda, R.; Sato, H.; Takata, M.; Kitagawa, S. Cellulose Hydrolysis by a New Porous Coordination Polymer Decorated with Sulfonic Acid Functional Groups. *Adv. Mater.* **2011**, *23*, 3294–3297.
- (46) Juan-Alcañiz, J.; Gielisse, R.; Lago, A. B.; Ramos-Fernandez, E. V.; Serra-Crespo, P.; Devic, T.; Guillou, N.; Serre, C.; Kapteijn, F.; Gascon, J. Towards Acid MOFs – Catalytic Performance of Sulfonic Acid Functionalized Architectures. *Catal. Sci. Technol.* **2013**, *3*, 2311–2318.
- (47) Yang, J.; Zhao, Q.; Li, J.; Dong, J. Synthesis of Metal–Organic Framework MIL-101 in TMAOH-Cr(NO<sub>3</sub>)<sub>3</sub>-H<sub>2</sub>BDC-H<sub>2</sub>O and Its Hydrogen-Storage Behavior. *Microporous Mesoporous Mater.* **2010**, *130*, 174–179.
- (48) Sene, S.; Marcos-Almaraz, M. T.; Menguy, N.; Scola, J.; Volatron, J.; Rouland, R.; Grenèche, J.-M.; Miraux, S.; Menet, C.; Guillou, N.; Gazeau, F.; Serre, C.; Horcajada, P.; Steunou, N. Maghemite-NanoMIL-100(Fe) Bimodal Nanovector as a Platform for Image-Guided Therapy. *Chem* **2017**, *3*, 303–322.
- (49) Zhao, X.; Wang, K.; Gao, Z.; Gao, H.; Xie, Z.; Du, X.; Huang, H. Reversing the Dye Adsorption and Separation Performance of Metal–Organic Frameworks via Introduction of –SO<sub>3</sub>H Groups. *Ind. Eng. Chem. Res.* **2017**, *56*, 4496–4501.
- (50) Marques, H. M.; Baldwin, D. A.; Pratt, J. M. Hemes and Hemoproteins. 3. the

- Reaction of Microperoxidase-8 with Cyanide: Comparison with Aquocobalamin and Hemoproteins. *J. Inorg. Biochem.* **1987**, *29*, 77–91.
- (51) Qi, P. X.; Beckman, R. A.; Wand, A. J. Solution Structure of Horse Heart Ferricytochrome c and Detection of Redox-Related Structural Changes by High-Resolution <sup>1</sup>H NMR. *Biochemistry* **1996**, *35*, 12275–12286.
- (52) Weckhuysen, B. M.; Wachs, I. E. *In Situ* Raman Spectroscopy of Supported Chromium Oxide Catalysts: <sup>18</sup>O<sub>2</sub> – <sup>16</sup>O<sub>2</sub> Isotopic Labeling Studies. *J. Phys. Chem. B* **1997**, *101*, 2793–2796.
- (53) Lefevre-Groboillot, D.; Dijols, S.; Boucher, J.-L.; Mahy, J.-P.; Ricoux, R.; Desbois, A.; Zimmermann, J.-L.; Mansuy, D. *N*-Hydroxyguanidines as New Heme Ligands: UV–Visible, EPR, and Resonance Raman Studies of the Interaction of Various Compounds Bearing a CNOH Function with Microperoxidase-8. *Biochemistry* **2001**, *40*, 9909–9917.
- (54) Othman, S.; Le Lirzin, A.; Desbois, A. A Heme C-Peptide Model System for the Resonance Raman Study of c-Type Cytochromes: Characterization of the Solvent-Dependence of Peptide-Histidine-Heme Interactions. *Biochemistry* **1993**, *32*, 9781–9791.
- (55) Karu, T. I.; Pyatibrat, L. V.; Kolyakov, S. F.; Afanasyeva, N. I. Absorption Measurements of a Cell Monolayer Relevant to Phototherapy: Reduction of Cytochrome c Oxidase under near IR Radiation. *J. Photochem. Photobiol. B* **2005**, *81*, 98–106.
- (56) Chen, Y.; Han, S.; Li, X.; Zhang, Z.; Ma, S. Why Does Enzyme Not Leach from Metal–Organic Frameworks (MOFs)? Unveiling the Interactions between an

- Enzyme Molecule and a MOF. *Inorg. Chem.* **2014**, *53*, 10006–10008.
- (57) de Lauzon, S.; Mansuy, D.; Mahy, J.-P. Coordination Chemistry of Iron (III)–Porphyrin–Antibody Complexes. *Eur. J. Biochem.* **2002**, *269*, 470–480.
- (58) Kadnikova, E. N.; Kostić, N. M. Oxidation of ABTS by Hydrogen Peroxide Catalyzed by Horseradish Peroxidase Encapsulated into Sol–Gel Glass.: Effects of Glass Matrix on Reactivity. *J. Mol. Catal. B Enzym.* **2002**, *18*, 39–48.
- (59) Patra, S.; Sene, S.; Mousty, C.; Serre, C.; Chaussé, A.; Legrand, L.; Steunou, N. Design of Laccase–Metal Organic Framework-Based Bioelectrodes for Biocatalytic Oxygen Reduction Reaction. *ACS Appl. Mater. Interfaces* **2016**, *8*, 20012–20022.
- (60) Kamata, K.; Hirano, T.; Ishimoto, R.; Mizuno, N. Sulfoxidation with Hydrogen Peroxide Catalyzed by  $[\text{SeO}_4\{\text{WO}(\text{O}_2)_2\}_2]^{2-}$ . *Dalton Trans.* **2010**, *39*, 5509–5518.
- (61) Kobayashi, S.; Nakano, M.; Kimura, T.; Schaap, P. A. On the Mechanism of the Peroxidase-Catalyzed Oxygen-Transfer Reaction. *Biochemistry* **1987**, *26*, 5019–5022.